19th Australasian Fluid Mechanics Conference
Melbourne, Australia
8-11 December 2014

Microbubble Generation in a Confined Radial Jet

P.A. Brandner, K.L. de Graaf, B.W. Pearce and J.S. Burgess

Australian Maritime College
University of Tasmania, Launceston, Tasmania 7250, Australia

Abstract

Microbubbles generated from the expansion of water supersaturated with dissolved air through a confined radial jet are investigated. Cavitation occurrence in the small-scale turbulent structures combined with gaseous diffusion promotes the formation of microbubbles. The effects of varying geometry, cavitation number and dissolved gas level are investigated to examine the cavitation physics and flow regimes resulting. The base of the radial jet is glass, enabling optical access for photographing the cavitation and microbubbles produced. The instantaneous extent of the main cavity volume is investigated using still photography. This is a preparatory study for later measurements of bubble production rate and size spectra.

Introduction

Microbubbles are used in a range of processes including flotation in minerals processing and waste water treatment [11], as contrast agents and vectors for local, triggered therapeutic delivery in medical applications [10], for sonication in sonochemistry [12], as nuclei in cavitation research [2] and for diagnostic tracers in liquids where solid particles are undesirable. The latter two applications are of interest for the present work.

The variable pressure water tunnel, or cavitation tunnel, within the Cavitation Research Laboratory (CRL) [1] at the Australian Maritime College incorporates microbubble generators for the above mentioned purposes. These are required for seeding the test flow with nuclei for modelling the inception and dynamic character of the hydrodynamic cavitation. The CRL tunnel also has separate arrays of microbubble generators for the purposes of seeding the flow for particle imaging velocimetry or particle tracking velocimetry. Microbubbles are preferred over solid seeding because of the large volume of water in the tunnel (365 m^3), the requirement for the water to contain no contaminants for the operation of ancillary equipment and the strict requirement to avoid potential sources of nucleation other than microbubbles. Separate arrays of devices are required for these two applications due to the quite different requirements of each. Microbubble populations typically required for artificial seeding of the test flow with cavitation nuclei range in diameter from 10 to 100 µm, both mono- and poly-disperse, at concentrations ranging from 0.01 to 10 per cm^3, over relatively large regions of the test flow. Conversely those for flow diagnostics require ideally mono-disperse diameters of order 10 µm, at concentrations of order 10 per mm^3, typically within a plane if illuminated with a laser sheet. These requirements dictate devices for the purposes of nuclei generation that produce order 10^5 bubbles/s and for the diagnostics 10^8 bubbles/s or greater. These large differences in production rate then require quite different devices.

Lab-on-chip devices [3,7,10] have recently undergone considerable development but typically require special considerations for management of surface energy of the liquid-solid-gas system making them impractical at this time. The devices currently used in the CRL and being further developed for nuclei and diagnostic purposes are those based on rapid expansion of supersaturated gas [2]. Devices based on this principle are reported on by [4] as being adaptable to produce flow rates varying over several orders of magnitude and thus offer the most promise for development of dedicated devices for each of these contrasting requirements. The CRL also has existing ancillaries for large volume production of supersaturated water required for microbubble production for degassing of the tunnel water.

The devices previously used in the CRL tunnel have been reported on in [2] which under typical operating conditions produce 5×10^5 bubbles/s. These devices were developed to achieve the maximum seeding concentration for nuclei of 10 bubbles/cm^3 however they have been shown for the grid spacing installed to not produce homogeneous seeding. Therefore new devices are being developed with lower production rates to be arrayed on a closer grid spacing to achieve homogenous seeding.

This paper reports on preliminary work on a microbubble generation device capable of variable geometry as well as geometric scaling to achieve a large range of microbubble production rates and different bubble sizes. Experimental results on the flow regimes, physics of the cavitating flow and flow rates as a function of the geometry and operating conditions are presented. This work provides a basic understanding of the device behaviour prior to more detailed work on measurement of bubble size distributions and production rates.

Experimental Setup

The device investigated achieves a rapid expansion of supersaturated water via radial diffusion as shown in figure 1. The supersaturated water is introduced axially and with the initial radial motion cavitation forms due to induced separation from the sharp edge of the inflow exit. With the cavity formation the flow initially undergoes a contraction before the radial expansion. The shedding of the unsteady cavity closure produces small-scale turbulent structures which combined with gaseous diffusion promote microbubble formation.

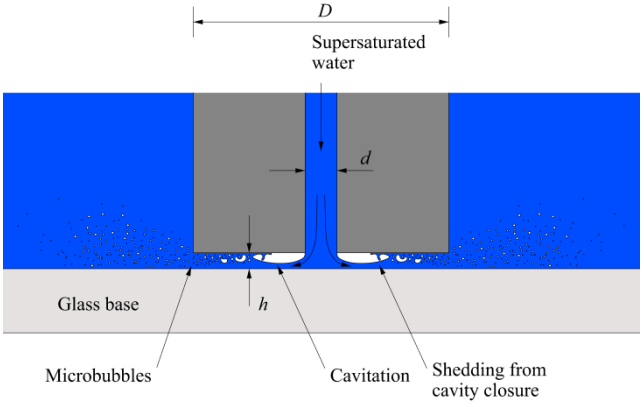

Figure 1. Schematic of the experimental setup showing the confined radial jet formed between the inlet nozzle and a glass wall permitting visualisation of the cavitation occurrence.

Figures 2 and 3 show typical plumes of the microbubbles generated. Figure 1 shows the geometric parameters of interest which may be expressed by the ratios D/d and h/d. The dimensionless parameters that characterise the flow include a cavitation number, $K = (p_2 - p_v)/(p_1 - p_2)$, a Reynolds number, $Re = Uh/\nu$, a Weber number, $We = \rho U^2 h/S$, and the saturation pressure ratio of the supply water, $SPR = p_{sat}/p_1$, where p_1 is the supply absolute pressure, p_2, the outlet absolute pressure, p_v, the vapour pressure, $U = Q/\pi dh$ the nominal throat velocity, Q, the flow rate, ρ, the density, ν, the viscosity, S, the surface tension and p_{sat}, the saturation pressure corresponding to the dissolved gas content. Nine generator nozzles have been made to study the effect of the geometric parameters, comprising 3 values each of d and D, as listed in Table 1. The nozzle faces were ground to a surface finish of 0.2 μm and the corners of the inlet and outlet maintained as nominally sharp edges. The nozzles were mounted on a micrometer stage to enable setting of the dimensionless height of the radial passage h/d, typically varied from 0 to 0.25. The nozzles are suspended from the micrometer stage above the floor of a glass tank enabling photographs to be taken of the microbubble plume from the side (figure 2) or from below to visualise the occurrence of cavitation (figure 3).

Figure 2. Side photograph of the generated microbubble plume from nozzle 3 for K = 0.13 and h/d = 0.08.

Figure 3. Photograph taken from below the glass base showing cavitation occurrence around the inlet nozzle periphery and the generated microbubble plume from nozzle 3 for K = 0.13 and h/d = 0.08.

Dimensionless parameters that typify nozzle operation are listed in Table 2. Typical throat velocities are about 25 m/s giving shedding frequencies of greater than $U/h \approx$ 250 kHz making these difficult to investigate by means other than high-speed photography which is planned for the future.Supersaturated water is supplied to the microbubble generator from a saturation vessel that may be pressurised to 2 MPa. To rapidly saturate an initially filled vessel an ancillary circuit is used. Vessel water is recirculated through a venturi with a perforated throat to ingest air from above the free surface enhancing the dissolution process. The saturation vessel pressure is measured using a Wika gauge pressure transducer Model P-10 with a precision of 0.1%. Atmospheric pressure is measured using a Vaisala Model PTB210 digital barometer with precision of ±0.03 kPa. The flow of supersaturated water to the microbubble generator is measured using the time rate of change of a level sensor from data acquired by a standard National Instruments/LabView data acquisition system. The level sensor is an Orion Instruments magnetically coupled liquid level sensor. The estimated precision of the microbubble generator flow rate measurement is < ±0.5%. The cavitation is photographed through the glass base using a Nikon 800E 35 mm digital SLR camera with a AF-S Micro NIKKOR 60 mm 1:2.8G ED lens.

Nozzle		D (mm)		
		6	7.5	9
d (mm)	0.5	1	2	3
	1.0	4	5	6
	1.5	7	8	9

Table 1. Summary of nozzle dimensions.

Parameter	*K*	*Re*	*We*	*SPR*
Value	0.25	2600	900	1.0

Table 2. Typical dimensionless parameters for nozzle 6 with p_1 = 500 kPa and p_2 = 100 kPa and h/d = 0.1.

Results

Figure 4 shows typical results of the cavitation occurrence for nozzle 6 at a fixed K value of 0.25 with increasing h/d. At small h/d values the flow is laminar with separated radial cavities that increase in number and circumferential periodicity with increase in h/d. This cellular nature would appear to be due to a combination of surface imperfections and capillary effects. The trailing edges of the radial cavities begin to destabilise and shed bubbles at about h/d = 0.04. These further destabilise with increasing h/d and begin to merge into a single annular cavity. With further increase the shedding zone grows eventually to the full cavity length at about h/d = 0.17, after which the cavity geometry remains constant through to h/d = 0.25. Figure 6 summaries the variation of cavity diameter, d_C, with h/d and shows the regions where the flow is laminar and where is has destabilised to turbulence and microbubble generation.

Figure 5 shows results for cavitation occurrence for nozzle 6 at fixed h/d = 0.1 with decreasing K. For each K value the dissolved gas content is at saturation at the supply pressure i.e. SPR = 1.0. At the high K values the flow appears similar to that for the small h/d values for the fixed K case shown in figure 4. With decreasing K the cavity diameter grows and the initial radial cells merge to form a less broken annular cavity. The cavity continues to grow with decreasing K until it reaches the outer diameter D of the nozzle at about K = 0.065, after which no further cavity growth results with decreasing K. In this case, unlike the fixed K case, the shedding zone remains a nominally constant length unaffected by the cavity growth.

A second test series was made with the dissolved gas content maintained at atmospheric pressure such that the SPR values varied from 0.5 for K = 1.0 through to about 0.06 for K = 0.0625. In this case the cavity behaviour is essentially the same as with the equilibrium saturated case except for slight changes in the cavity diameter variation with K. Figure 7 summarises the variation of cavity diameter, d_C, with K for both cases. For the higher K values the cavity length grows with a power law similar to many larger scale cavitation problems [9] but diverges from this behaviour as the cavity diameter approaches the nozzle outer diameter D.

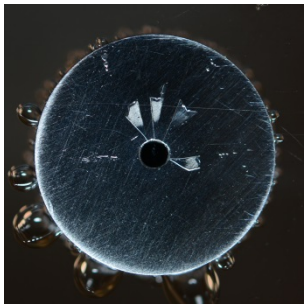

h/d = 0.01

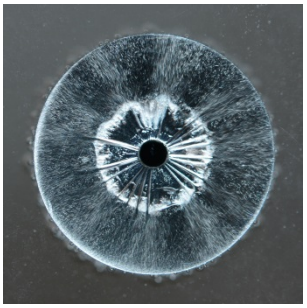

h/d = 0.07

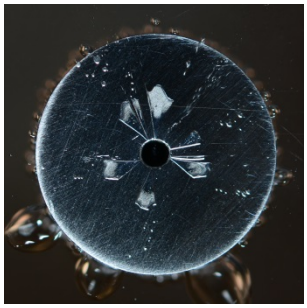

h/d = 0.02

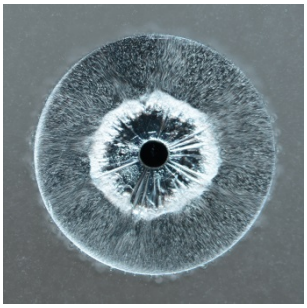

h/d = 0.09

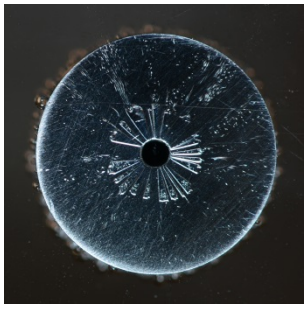

h/d = 0.03

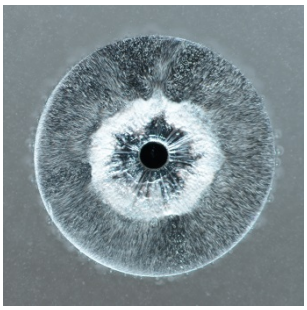

h/d = 0.11

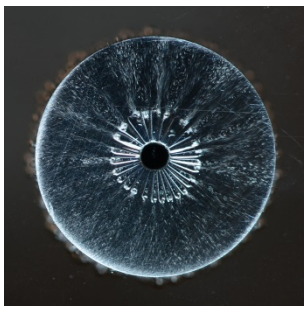

h/d = 0.04

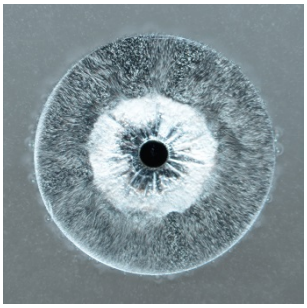

h/d = 0.13

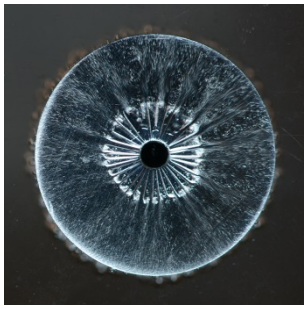

h/d = 0.05

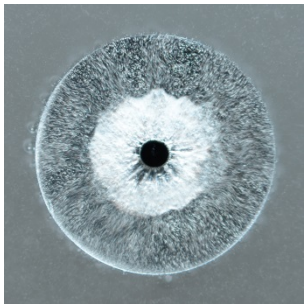

h/d = 0.17

Figure 4. Photographs of nozzle 6 cavitation development for K = 0.25 with increasing h/d.

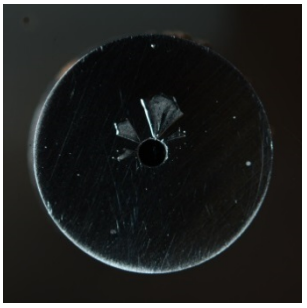

K = 0.98

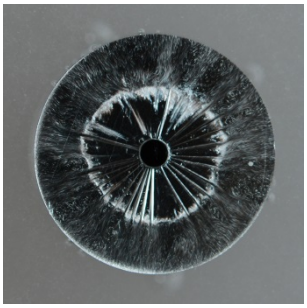

K = 0.163

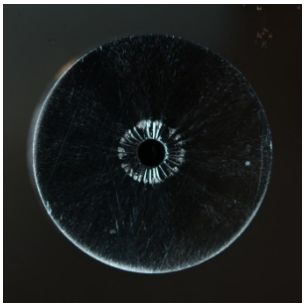

K = 0.49

K = 0.14

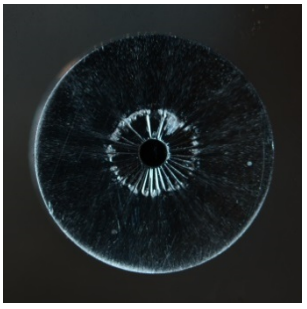

K = 0.327

K = 0.109

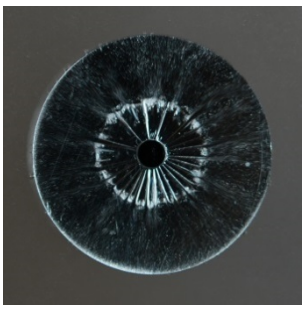

K = 0.245

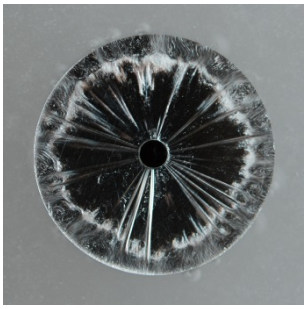

K = 0.089

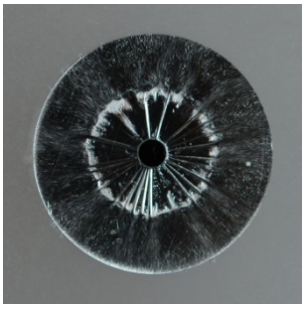

K = 0.196

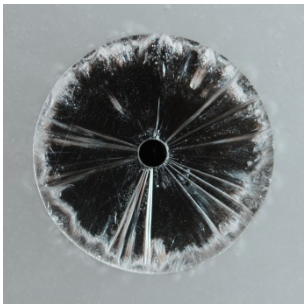

K = 0.065

Figure 5. Photographs of nozzle 6 cavitation development for h/d = 0.1 with decreasing K.

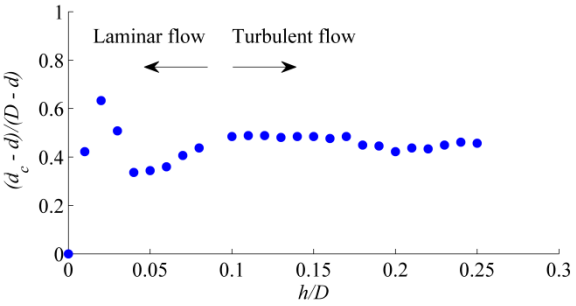

Figure 6. Variation of cavity diameter with h/d at K = 0.25 for nozzle 6 showing regions of laminar flow and where the cavities destabilise to turbulence and microbubble generation.

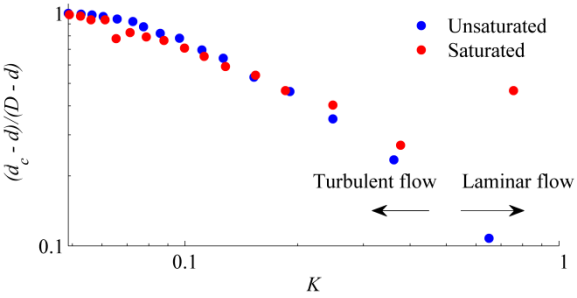

Figure 7. Variation of cavity diameter with K at h/d = 0.1 for nozzle 6 with water saturated at the supply pressure and with unsaturated water (atmospheric pressure) at showing regions of laminar flow and where the cavities destabilise to turbulence and microbubble generation.

The effect of cavitation on the flow through cylindrical macro- and micro-orifices has been studied extensively [5,6,8]. In many cases empirical observations on the flow geometry have been used to determine relations for determining when the flow becomes choked. Choked flow in this context is when the pressure at the vena contracta reaches vapour pressure resulting in no further increase in flow with decrease in downstream pressure. For the flow studied here there are no empirical observations on flow geometry and it is not practical to easily measure the pressure at the vena contracta or throat of the radial jet. However given the flow rate and the supply pressure the contraction coefficient, C_C may be derived assuming no loss (velocity coefficient of 1) by applying the usual Bernoulli and continuity equations between the supply and throat locations:

$$C_c = \frac{1}{\sqrt{\frac{2(\pi dh)^2(p_1 - p_v)}{\rho Q^2} + \frac{4dh}{D^2}}} \qquad (1)$$

The variation of C_C with K corresponding to the results presented in figure 7 is shown in figure 8. For unsaturated case the C_C is about 0.8 for the high K values similar to the discharge coefficient for many nozzles in un-choked or non-cavitating conditions but reduces with reduction of K suggesting the onset of choked conditions. The saturated case shows similar behaviour but with consistently lower C_C values. These lower values suggest a greater cavity volume and hence greater flow restriction due to the greater partial pressure of air from diffusion driven by high dissolved gas content in the saturated case.

Conclusions

Cavitation occurrence in a microbubble generator has been studied to gain insight into the flow physics and practical regimes of operation. Laminar flow results for small dimensions and high cavitation numbers such that cavitation instabilities do not form providing shedding and turbulent breakdown to generate microbubbles. The cavity diameter is unaffected by increase in passage height for a fixed cavitation number. The width of the shedding zone, however, grows with increasing in height eventually growing to the full cavity width. The cavity diameter grows with decrease in cavitation number for a fixed passage height eventually growing to the limiting value of the outside diameter of the nozzle. In this case the shedding zone remains nominally fixed in length unaffected by cavity growth. The results in both the case tested suggest the flow is choked for the lower cavitation numbers investigated.

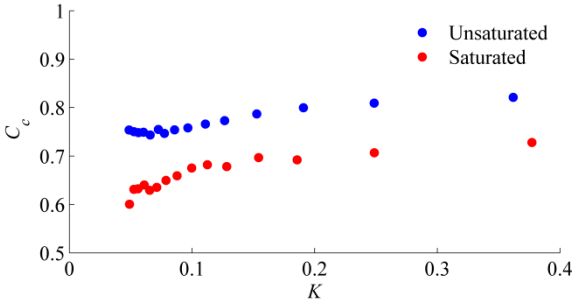

Figure 8. Variation of contraction constant, C_C with with K at h/d = 0.1 for nozzle 6 with water saturated at the supply pressure and with unsaturated water (atmospheric pressure) assuming choked flow conditions as per equation 1.

Acknowledgments

The authors wish to acknowledge the support of the DSTO and the University of Tasmania.

References

[1] Brandner, P.A., Lecoffre, Y. and Walker, G.J., Design Considerations in the Development of a Modern Cavitation Tunnel, *Sixteenth Australasian Fluid Mechanics Conference*, Gold Coast, Australia, 2007.

[2] Brandner, P.A., Wright, G., Pearce, B.W. Goldsworthy, L. and Walker, G.J., An Experimental Investigation of Microbubble Generation in a Confined Turbulent Jet, *Seventeenth Australasian Fluid Mechanics Conference*, Auckland, New Zealand, 2010.

[3] Hettiarachchi, K., Talu, E., Longo, M.L., Dayton, P.A. and Lee, A.P., On-chip generation of microbubbles as a practical technology for manufacturing contrast agents for ultrasonic imaging, *Lab on a Chip*, **7**, 2007, 463-468.

[4] Lecoffre, Y., *Cavitation Bubble Trackers*, A.A. Balkema, 1999.

[5] Lichtarowicz, A. and Pearce, I. D., Cavitation and aeration effects in long orifices. *Cavitation*, Edinburgh, The Institution of Mechanical Engineers, 1976, 129-144.

[6] Mishra, C. and Peles, Y., Cavitation in flow through a micro-orifice inside a silicon microchannel, *Physics of Fluids* **17**, 2005, 013601.

[7] Miyazaki, R., Ogasawara, T., Takeuchi, S. Takagi, S. and Matsumoto, Y., Scaling and dynamics of microbubble generation in microfluidic T-junction. *7th International Conference on Multiphase Flow - ICMF 2010*. Tampa, Fl, USA, 2010, paper 15.12.11.

[8] Nurick, W. H., Orifice cavitation and its effect on spray mixing, *Journal of Fluids Engineering*, **98**, 1976, 681-687.

[9] Pearce, B. and P. Brandner, Inviscid cavity flow over a wall-mounted fence, *Ocean Engineering*, **80**, 2014, 13–24.

[10] Peyman, S.A., Abou-Saleh, R.H., McLaughlan, J.R., Ingram, N., Johnson, B.R.G., Critchley, K., Freear, S., Evans, J.A., Markham, A.F., Coletta, P.L. and Evans, S.D., Expanding 3D geometry for enhanced on-chip microbubble production and single step formation of liposome modified microbubbles, *Lab on a Chip*, **12**, 2012, 4544-4552.

[11] Rodrigues, R.T. & Rubio, J., New basis for measuring the size distribution of bubbles, *Minerals Engineering.*,**16**, 2003, 757-765.

[12] Suslick, K. S. and Flannigan, D. J., Inside a collapsing bubble: sonoluminescence and the conditions during cavitation, *Annual Review of Physical Chemistry,* **59**, 2008, 659-683